Results in Physics 58 (2024) 107501

Contents lists available at ScienceDirect

Results in Physics

journal homepage: www.elsevier.com/locate/rinp

Learning in colloidal polyaniline nanorods

Alessandro Chiolerio [a,b,*], Erik Garofalo [a], Neil Phillips [b], Ermelinda Falletta [c], Rodrigo de Oliveira [a,d], Andrew Adamatzky [b]

[a] Bioinspired Soft Robotics, Istituto Italiano di Tecnologia, Via Morego, 30, 16163 Genova, Italy
[b] Unconventional Computing Laboratory, University of the West of England, Coldharbour Lane, BS16 1QY Bristol, UK
[c] Department of Chemistry, Università degli Studi di Milano, Via Golgi 19, 20133 Milano, Italy
[d] Universidade Estadual da Paraíba, Centro de Ciências e Tecnologia – CCT, Departamento de Química, Rua das Baraúnas, 351 – Bairro Universitário Campina Grande-Paraíba, CEP 58429-500, Brazil

ARTICLE INFO

Keywords:
Colloids
Nanorods
Learning
Liquid robotics
Nanomaterials

ABSTRACT

Liquid-based computing media are massively parallel computing devices with high fault-tolerance and self-healing capabilities. They can compute by propagating and interacting phase waves or by changing their internal coordination. Colloidal suspensions of conductive polymer nanorods are expected to be interesting candidates for developing the computing subsystem in such applications, because of their anisometry which makes them particularly susceptible to electrical fields. In this work, we investigated a suspension of polyaniline nanorods (NRs) to explore the potential of generating learning mechanisms in the colloid and applying them in the computing system of future cybernetic systems. We demonstrated that learning, as expressed in the formation of programmable conductive pathways leading to distinct states, can be implemented using Alternated Current (AC) electrical stimulation. We achieved repeatable programming of colloid resistance anisotropy that can be easily mapped into binary logic, demonstrating that this is due to the AC field effects on the hydrogen bonds that stabilise the dispersoids in the solvent as well as the charges' orientation inside the polymeric chains. We also influenced the conductivity of polyaniline (PANI) NRs by changing their molecular conformation. The findings establish robust protocols for programming future liquid robots.

Introduction

A harsh or extreme environment can be defined as a place that is hazardous to agents (humans or robots) exploring it, characterized by high levels of radiation, high explosive risk, extreme temperatures or pressures, corrosive and toxic chemicals and lack of oxygen, or as an environment that is challenging for agents to operate in, like remote, unknown, cluttered, dynamic, unstructured and limited in visibility [1]. In the recent years, advancements in materials science and cybernetic technology in the field of Smart Fluid Systems (SFS) show that, compared to conventional robotic systems, liquid or colloid-based robots would offer advantages in terms of versatility, adaptability, resiliency, mobility, distributed architecture and autonomy especially for applications in harsh environments, such as gas giants, comets and asteroids, or deep-sea and post-earthquake areas for search and rescue applications [2,3] but also for oil and gas pipes and nuclear waste inspections [4]. A smart fluid (SF) is defined as a liquid-state system featuring unprecedented properties thanks to the cooperation of two phases, usually a fine solid phase dispersed in a solvent at the liquid or gaseous state, whose single constituents enable smart distributed functionalities such as information processing capabilities, self-powering, sensing capabilities and mobility [2]. Thus, complex systems based on SF, named SFS, represent a new paradigm in the field of cybernetic systems, combining the versatility of conventional robotics and the advantages of soft robotics. In fact, the latter, based on highly compliant materials like those found in living organisms, offers innovative solutions, especially in terms of mobility, showing little resistance to compressive forces and consequently, conforming to obstacles and squeezing through openings smaller than their nominal dimensions. Additionally, SFS could exploit the collective properties of its constituents, relying on the variation of its main physical properties such as shape, viscosity, thermal conductivity, magnetic permittivity and permeability, electrical conductivity, magnetization, among other ones [2], to execute basic robotic operations. The capabilities of SFS in the

* Corresponding author at: Center for Convergent Technologies – Bioinspired Soft Robotics Istituto Italiano di Tecnologia, Via Morego, 30, 16163 Genova, Italy.
E-mail addresses: alessandro.chiolerio@iit.it (A. Chiolerio), erik.garofalo@iit.it (E. Garofalo), neil.phillips@uwe.ac.uk (N. Phillips), ermelinda.falletta@unimi.it (E. Falletta), deoliveirarj@servidor.uepb.edu.br (R. de Oliveira), andrew.adamatzky@uwe.ac.uk (A. Adamatzky).

https://doi.org/10.1016/j.rinp.2024.107501
Received 22 August 2023; Received in revised form 3 January 2024; Accepted 19 February 2024
Available online 24 February 2024

areas of energy generation [5], energy storage, information collection, storage, and transmission, sensing [6], and mobility have been assessed and some experimental milestones were achieved, esp. on the energy generation system [7–11]. Therefore, since liquid robotics, in response to the future increasingly distributed sensing and resulting data to be managed, has been proposed as the next cybernetic solution, the next step should further explore the ability of storing and elaborating information by using electrically reconfigurable SF [12]. Thus, following original ideas of a liquid controller for robots [13] and the recent advances in the field of unconventional computing [14–16], this work aims at investigating the capability to create pathways in a suspension of electrically conductive polymeric nanorods in a polar liquid when stimulated by an electric field, in order to explore the potential of generating learning mechanisms in the colloid and applying them in the memorization and computing system of future robots. The consolidated Von Neumann computer architecture is such that the memory is kept separated from the Central Processing Unit (CPU) and this is reflected by the sequential operation, allowing instructions to be processed one at a time, which strongly impacts on the performance of parallel processing [17]. Next generation computing systems are being developed by using neuromorphic devices, in other words synthetic synapses mimicking the plasticity features of biological brains that enable learning: a change in the transfer function of any agent as a consequence of particular input conditions (i.e. amplitude, repetition, and so on). Resistive switching (learning) induced by AC stimuli of colloids could theoretically be employed to enable massively parallel computing [18]. We prepared and characterized polyaniline (PANI) nanorods (NRs) and we dispersed them in ethanol. Then, we designed a customized setup for the learning experiments, conceived to easily apply an electric stimulus to the liquid and simultaneously measuring its electrical resistance in parallel and perpendicular direction with respect to the stimulus axis, and developed a numerical simulation to better visualize the topology of the electrical field experienced by the colloid.

Materials and methods

PANI nanorods: synthesis and characterization

All the materials employed in the synthesis were purchased from Merck and used without any pre-treatment process. PANI NRs were synthesized by a template-free method reported by Jang et al. with some modification [19]. 1 g of aniline was dissolved in 100 mL of 0.6 M acetic acid (CH_3COOH/Aniline = 6 M ratio) at room temperature. Then, 2.9 g of $FeCl_3{\cdot}6H_2O$ (Fe^{3+}/aniline = 0.6 M ratio) were added into the solution followed by 2.5 g of ammonium persulfate, APS, (APS/Aniline = 1 M ratio). After 3 h, the reaction was stopped by the addition of ethanol. The solid product was collected by filtration, washed several times by ethanol and dried overnight in air. PANI/CH_3COOH NRs were obtained with a yield higher than 98 %. PANI/CH_3COOH NRs were characterized through ultraviolet–visible (UV–vis) spectroscopy, Fourier transformed infrared (FT-IR) spectroscopy, X-ray powder diffraction (XRPD), X-ray photoelectron spectroscopy (XPS) and scanning electron microscopy (SEM). UV–vis spectra were acquired in the range 200–800 nm by a Hewlett Packard HP8453 spectrophotometer. A few milligrams of the compound was dissolved in N,N-dimethylformamide (DMF) by ultrasonic irradiation for 15 min and then filtered with PTFE 0.4 μm syringe filter. Then, the resulting organic dispersion was analyzed. FT-IR (KBr disk technique) and ATR-FTIR spectra were performed using a Jasco FT-IR 410 spectrophotometer in the range 400–4000 cm^{-1}. XRPD diffractograms were carried out by a Rigaku D III-MAX diffractometer equipped with a Cu lamp in the range of 5–80 2 theta [°]. Surface composition of samples was studied by X-ray photoelectron spectroscopy (XPS) by means of an M−PROBE Surface Spectrometer with an Al (Kα) source and a spot size from 0.15 mm to 1 mm in diameter (USA). A 10 V applied voltage at a vacuum of 10^{-7} –10^{-8} Torr was used. Survey scans were investigated in 0—–1100 eV binding energy range, using a spot size of 800 μm with 4 eV energy resolution (scan rate of 1 eV per step). ESCA Hawk Software was used for data curation. Charge neutralization was carried out by means of a low-energy electron beam. In any case, the resulting binding energy values (BE) were corrected by setting the C 1 s peak (C–C) fixed at 284.6 eV as the reference. The samples morphology was investigated by scanning electron microscopy (SEM), performed on a FE-SEM Sigma (Zeiss). No golden-coated sample wase observed at 2.5 kV of HT.

Microelectrodes array setup

To investigate the learning phenomena in PANI NRs, an appropriate setup was needed. We found that a microelectrode array (MEA) with some ad hoc modification was suited to the purpose since it allowed to apply an electric field of about 12.8 kV/m with a signal of 10 V between two printed electrodes spacing 0.78 mm, similarly to what found in other works [20]. MEA is a customised printed circuit board (PCB), shown in Fig. 1 where two close-up views are provided. To perform the experiments, a cylindrical container is sealed with epoxy resin in the central testing region so that the about 2 mL of PANI NRs dispersion can fit into it being in contact with the microelectrodes array.

The testing circular area measures about 6.4 mm in diameter. A specific lid was 3D printed to keep in place 4 needle electrodes measuring 0.75 mm in diameter, spacing 2 mm and in contact with the colloid, to perform the resistance measures in the directions parallel and perpendicular to the electric field applied for stimulating the PANI NRs. In Fig. 2, the 3D model of the final setup is shown.

Experiments description

The tests on learning behaviour were conducted employing a PANI NRs dispersion in ethanol with a concentration of 1 % in weight. The density of PANI is 1.3 g cm^{-3} (Sigma-Aldrich commercial products), leading to a packing fraction of 0.58 %, which stands below the percolation threshold. An AC electrical signal was applied to stimulate the PANI NRs colloids by means of a GW Instek function generator connected to a pair of printed electrodes on the MEA, spacing 0.78 mm. The signal was a sinusoidal wave with an amplitude equal to 10 V and frequencies 1, 10, 100 and 1000 kHz. Two pairs of platinum needles were used to perform resistance measurements in the direction parallel and perpendicular to the applied electric field lines. Each pair of electrodes has two needles spacing 2 mm. The testing area was filled with 2 mL of colloidal PANI, creating a disk-shaped volume with a thickness of 1 mm, to just cover the electrodes and without generating a 3D setup. Then, the DC resistance in both directions was measured simultaneously for 2 min with a Semiconductor Characterization System SCS4200 from Tektronix equipped with two independent sample measurements units, with a true sampling rate of 170 ms. We performed a first acquisition of 2 min before applying the stimulus, then the function generator was switched on for 1 min after an initial settling time and the resistance was measured again for 2 min. Finally, the function generator switched off, the resistance was measured after applying the stimulus for 2 more minutes. The test was repeated 5 times at each investigated frequency, using a freshly made colloid sample every time, to avoid eventual systematic errors due to partial solvent evaporation, unwanted sample heating, electrostatically induced sample aggregation. Fast experiments, conducted immediately after submitting AC stimuli, were performed on the colloids using FT-IR (as above described) and impedance spectroscopy (Agilent E4980A precision LCR meter) in the range from 100 Hz to 1 MHz with a signal of 100 mV amplitude.

Green laser alignment measurements were performed using a green diode emitting at 532 nm with a steady power of 5 mW (shown in the Supporting Information).

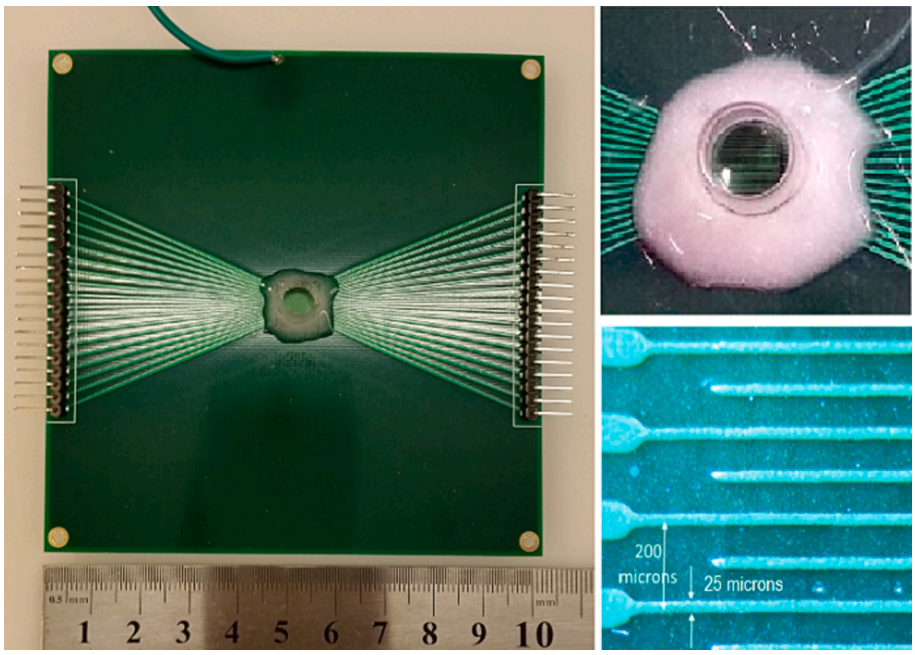

Fig. 1. Picture of MEA with close-up views.

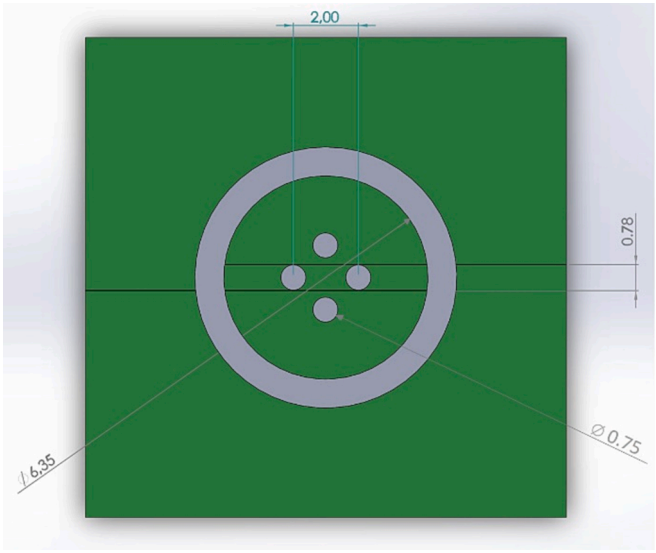

Fig. 2. Top view of 3D model of the experimental setup (dimensions in mm).

COMSOL model description

The 3-dimensional FEM model (shown in the Supporting Information) features 126,759 elements, a free meshing time of 1.80 s, the number of degrees of freedom solved of 202730. The stationary Solver used processed the boundary conditions providing the solution in 2731 s, running with a physical memory of 1.11 GB and virtual memory of 1.26 GB, on an Intel® Core™ i5-4590 CPU @ 3.30 GHz equipped with 16 GB RAM.

Results and discussion

PANI nanorods characterization

The synthesized PANI NRs were characterized by several techniques and the results are reported below. Fig. 3 shows the Fourier Transform InfraRed (FT-IR) of the dried NRs and the UV–vis spectra, as well as the XRPD pattern and the XPS investigations.

Both FT-IR and UV–vis spectra of the sample exhibit the typical bands of PANI in form of emeraldine salt. Concerning FT-IR investigations, the broadband centered at 3446 cm^{-1} can be related to the N-H stretching vibration mode, as studied by Abdelraheem et al [21]. The C = C stretching vibration of quinoid (Q) and benzenoid (B) rings are responsible of the bands at 1569 and 1489 cm^{-1} respectively, whereas the band at 1311 cm^{-1} can be assigned to the secondary aromatic amine C–N stretching vibration modes.

The band at 1240 cm^{-1} confirms the presence of C–N+• stretching vibration, and that at 1146 cm^{-1} is due to Q = NH + –B, B–NH + –B stretching, numerically near to the NH···N interchain hydrogen bond observed at 1116 cm^{-1}. These positive charges on aniline units are balanced by negatively charged counterions, typically chloride, depending on the doping agent used (here acetate ions), to maintain the electro-neutrality of the polymer surface [22]. The bands in the range 820–800 cm^{-1} can be attributed to C–H out-of-plane bending vibrations of 1,4-disubstituted aromatic rings. Finally, the presence of C–H vibrations of 1,2,4-trisubstituted and 1,2-disubstituted rings can be inferred from the two bands at 800 and 759 cm^{-1} respectively [23]. The entity of the ratio (*ca.* 1) between the FT-IR bands at 1570 cm^{-1} and that at 1490 cm^{-1} (quinoid and benzenoid band, respectively), as well as the intensity of the band at ca. 1146 cm^{-1} (electronic like band) are strictly related to the conductive behavior of the polymer [24], demonstrating that PANI NRs were obtained in their conducting form of emeraldine salt (half-oxidized and half-protonated structure). It can be observed from the Fig. 7 B that the colloids explored in the learning experiments still present these main infrared absorption bands, even if some displacement is observed, showing that chemical bonds in the PANI were preserved. All of the main stretching/vibration peaks have been assigned and listed in Table S1.

The UV–Visible absorption spectrum of PANI depends on several factors: level of doping, extent of conjugation, solvent, etc. [25]. As expected [26–28], the UV–vis spectrum of dried PANI NRs acquired in DMF solution contains the typical bands of deprotonated emeraldine base (Fig. 3 B), owing to the deprotonation/dedoping effect of the solvent [29]. More in detail, the band at 275 nm can be attributed to π-π* conjugated ring system, whereas polaron π* and polaron π transitions

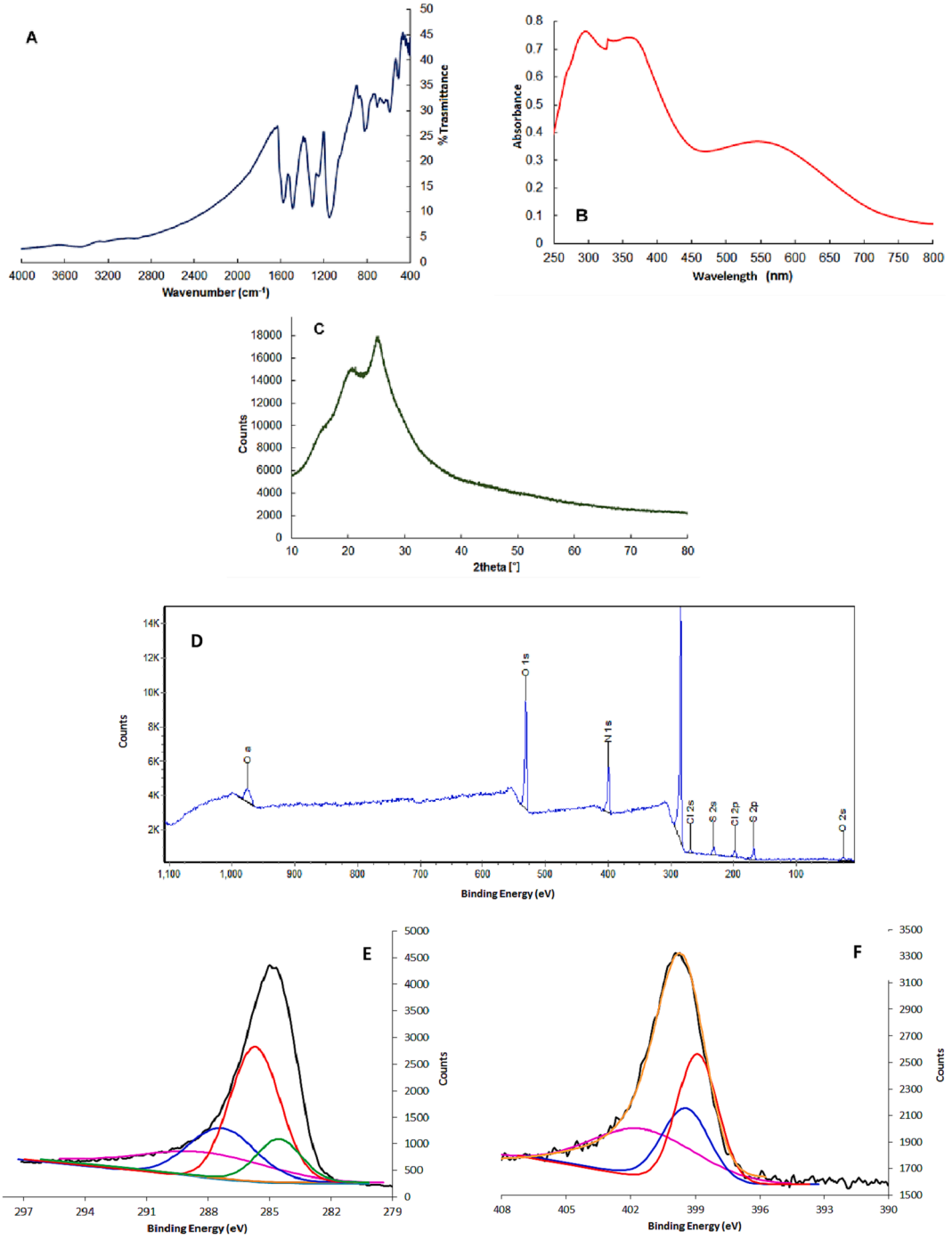

Fig. 3. A) FT-IR spectrum, B) UV–vis spectrum, C) XRD pattern, D) XPS survey spectrum, E) XPS HR C1s spectrum, F) XPS HR N1s spectrum of PANI nanorods.

are responsible for the band at 365 nm and 570 nm respectively, that confirms the emeraldine salt form of the polymer [30]. In addition, also the XRPD pattern (Fig. 3 C) of the sample confirms that the PANI NRs were successfully synthesized in form of conducting powder. In particular, the diffraction depicted in Fig. 3 C are typical of emeraldine salt in ES-I form [31]. The three main peaks at 2theta = 15°, 20° and 25° correspond to (011), (020) and (200) crystallographic planes reflections of emeraldine salt and are related to the repeat unit of the PANI chain and to their periodicity perpendicular and parallel.

Finally, XPS was employed to investigate the surface elemental composition and chemical state of PANI. The XPS survey (Fig. 3 D) exhibits peaks related to S, Cl, as well as C and N. If on the one hand the presence of Cl can be ascribed to the use of $FeCl_3$ during the polymer synthesis, on the other hand the peak of S is related to the used oxidizing agent (APS) that during the oxidative polymerization of aniline is converted into sulphate, whereas no peaks related to the presence of iron are observed.

Many researchers have been demonstrated the positive effect of S-doping in the structure or on the surface of the polymer towards their electrochemical performance [32,33].

The high-resolution (HR) XPS spectra of C 1 s and N 1 s are displayed in Fig. 3 E and F, respectively. The HR spectrum of C 1 s (Fig. 3 E) can be deconvoluted into three components at 284.4, 285.6, 287.4 and 288.7 eV ascribed to C–C/C–H, C–N, C = N, and π-π (satellite), respectively [34]. Fig. 3 F displays the HR XPS spectrum of N 1 s, which can be curve-fitted into three peaks at 398.8, 399.4 and 401.7 eV related to the

presence of imine structures, neutral amine, and cationic nitrogen atoms (N^+) [34,35].

The morphology of the sample was investigated by SEM microscopy and the results are reported in Fig. 4 A and B, while Fig. 4 C shows the histogram with NR diameter distribution.

The obtained material consists of a tangled network of nanorods with a narrow distribution of the diameters centered at 47 nm (Fig. 4 F). In contrast, the length is difficult to measure. However, they are in the order of hundreds of nm, although the magnetic stirring applied during their preparation causes a partial break of the nanomaterials.

The NRs formation can be attributed both to the use of a combined oxidation system (APS/Fe^{3+}), that leads to a rapid mixing polymerization reaction that has a strong influence on the polymer morphology [36], and to the use of acetic acid as the doping agent. It has been demonstrated that PANI formation includes three steps: the induction period, the formation of pernigraniline and the reduction of pernigraniline to the emeraldine [37]. In the first step, the induction period, the formation of oligomers is strongly related to the oxidizing species employed. The high oxidation capability of the APS/Fe^{3+} combined system guarantees the production of substantial number of oligomers in the initial period, that produce the final NR structures by self-assembly processes. Even though the effect of the type of doping agent on the final morphology is not completely clear, it has been observed that the initial polymerization step, initiation, favourably occurs under low ionic strength, due to the use of weak acids, with a positive effect on the production of wires and rods [38].

It is worth noting that in contrast to solid systems, in a colloid several aspects must be taken into consideration, because its behaviour is governed not only by particle–particle but also by particle–solvent interactions. In this regard, De Medeiros et al. investigated electrostatic interactions of the polymer by surface particle charges by potential investigations on doped PANI [39], reporting for PANI positive values of potential in water, indicating that the polymer acquires positive charges because of doping.

The solvent used for the polymer dispersion plays a role also in the specific conductivity which depends on the oxidation level of the polymer and on the degree of protonation (primary doping) but also on the presence of substance that indirectly affect the charges separation on the polymeric backbone and consequently the chains conformation (secondary doping) [40]. However, as reported in the literature, the conductivity value for PANI-based materials is function of several other factors, such as humidity, type of dopants and doping level, among others [41].

Tarachiwin et al. investigated the specific conductivity of HCl-doped and CH_3COOH-doped polyaniline films, demonstrating for CH_3COOH-doped PANI values of conductivity lower than for HCl typical of semiconductor materials, but less sensitive to the ethanol concentration. However, a positive increment upon exposure to water and ethanol was observed and was attributed to an increased electron mobility upon exposure to the solvent due to an enhanced interchain H-transfer [42].

Learning tests

The tests conducted on the PANI NR dispersion lasted in total 6 min and are divided in 3 distinct phases along which the DC resistance parallel to the direction of the stimulus electric field ($R_{//}$) and the perpendicular one (R) are measured simultaneously. An exemplar comparison between the parallel resistance measurements before, during and after a stimulus provided at 1 kHz is shown in Fig. 5 A. After a settling time of approximately 20 s, the resistance reading becomes steady in the 5 MΩ range (black curve). The effects on resistance of the application of the electrical stimulus at 1 kHz is monitored by the red curve, and the timing of the signal generator is tracked by the dashed line on top of the graph, lasting approximately 1 min. The stimulus provokes a strong reduction of the parallel resistance of about two orders of magnitude that lasts 40 s, then we notice a fast and discontinuous growth of the resistance that keeps recovering and also surpassing the initial resistance values after the signal generator is switched off. This first observation justifies the fast experiments conducted by combining FT-IR and impedance spectroscopy, to better explore this fast relaxation,

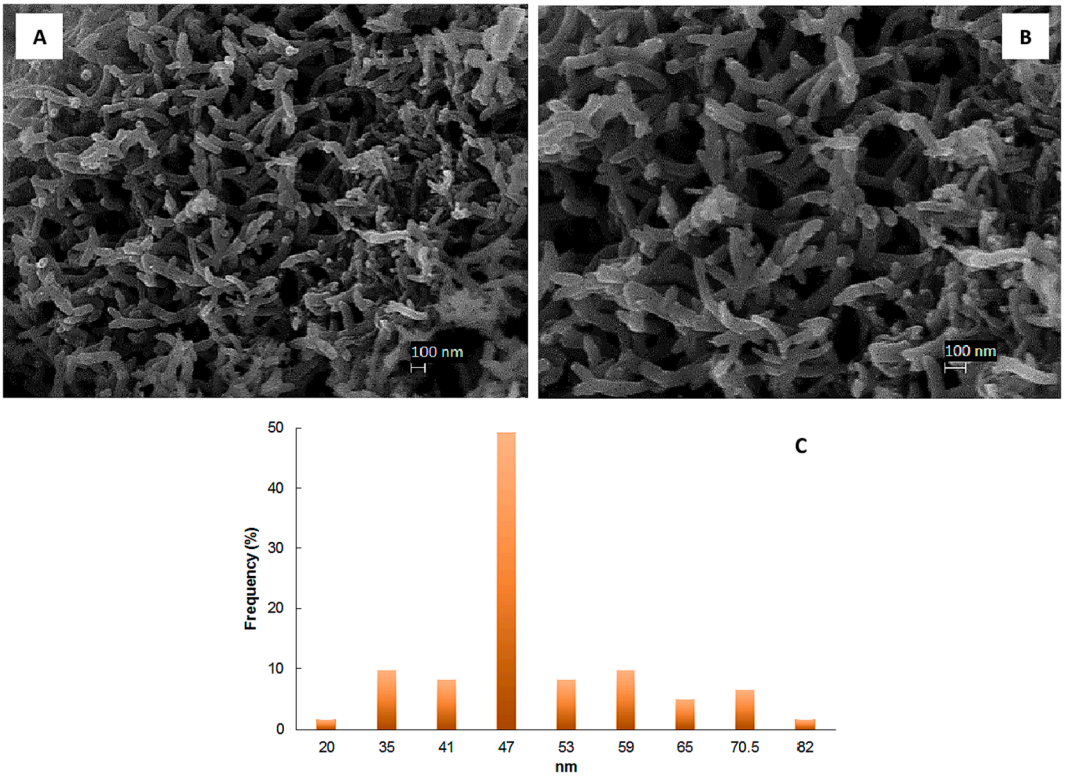

Fig. 4. (A, B) SEM images and (C) diameter distribution of PANI NRs.

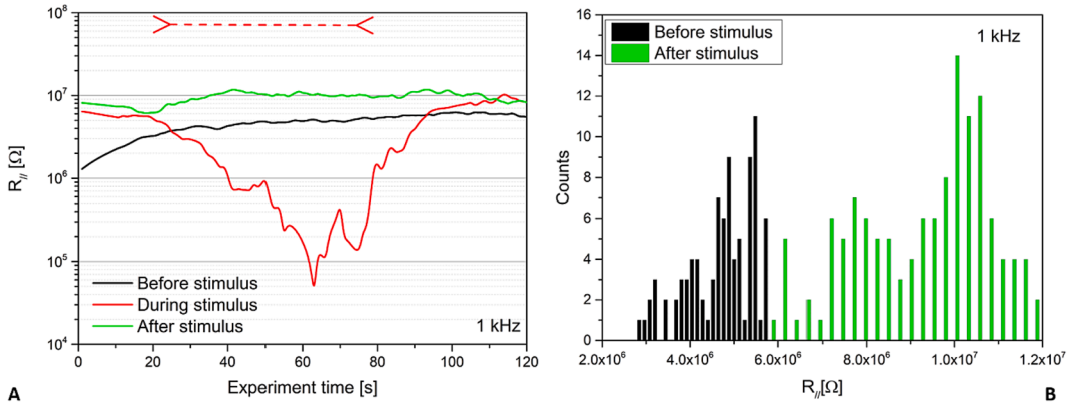

Fig. 5. (A) Parallel resistance measurements before (black), while (red), and after (green) the sample was submitted to a stimulus @ 1 kHz. The red arrow on top of the graph shows the exact timing when the stimulus was switched on and off during the recording of the "During stimulus" curve. (B) statistics of the parallel resistance distributions before and after the stimulus. (For interpretation of the references to colour in this figure legend, the reader is referred to the web version of this article.)

described below. In fact, the third curve (green) shows what happens after the stimulus has been applied, where the DC parallel resistance settles around a value of 10 MΩ. By extracting statistical data from the black and green curves, respectively before and after the stimulus was applied, we can plot the histograms shown in Fig. 5 B: the two average values are clearly distinguishable, and the two distributions are close but not overlapped. This is the first basic requirement to build up a binary memory system. Similar measurements were performed also at a frequency of 10, 100 and 1000 kHz, generating the aggregated data presented in Table 1, while relevant graphs have been placed in the Supporting Information file for completeness (Fig. S2-4). For each frequency, experiments have been repeated five times, to ensure the good repeatability of the phenomena; moreover, all data were treated in a fully consistent statistical manner, calculating the error (standard deviation) and performing error propagation over derived quantities. The most relevant parameter, to evaluate colloid conductivity anisometry induced by the effects of the oscillating electric field used as stimulus, is the relative DC resistance anisotropy defined by Equation (1):

$$R_a = \frac{R_{//} - R_{\perp}}{R_{//}} \tag{1}$$

We have the following notable ideal cases: $R_a = 1$ when $RT = 0$, in other words the system under evaluation has infinite conductivity in the direction orthogonal to the stimulating electric field; $R_a \rightarrow -\infty$ when $R_{//}=0$, in other words the system under evaluation has infinite conductivity in the direction parallel to the stimulating electric field; $R_a = 0$ when $R_{//}= RT$, in other words the system is perfectly isotropic across the characterization plane. Furthermore, we have that: $R_{//} \gg RT \rightarrow R_a \rightarrow 1$ and $RT \gg R_{//} \rightarrow R_a \rightarrow -RT$. Looking at Table 1 entries, a dispersion of values before the stimulus is applied can be found, but a generalised property is that $R \gg R_{//}$; given the geometry of the sample holder, we can suppose that the measurement device can by itself produce a measuring current and electric field distribution that is already able to provide a source of anisotropy, enhancing the DC conductivity of the parallel path. After the application of the stimulus, we have two different cases: the low frequency limit (1 and 10 kHz) where after the stimulus we approach a more isotropic situation, and the high frequency limit (100 and 1000 kHz) where after the stimulus we confirm or enhance the higher conductivity of the parallel channel. In the former case, the effect of the electric field is that of destroying the order that favours conductivity along the parallel direction; in the latter case, the effect of the electric field is that of reinforcing such order, particularly at 1 MHz.

Table 1
Comparison of R_a values derived from experiments, before and after submitting the stimulus.

Frequency [kHz]	Before stimulus	After stimulus	Minimum Distance [MΩ]
1	−1.9 ± 0.5	−0.2 ± 0.02	1.198
10	−1.1 ± 0.5	−0.4 ± 0.1	0.1
100	−3.3 ± 0.7	−3.3 ± 0.5	Overlapped
1000	−1.9 ± 0.9	−3.1 ± 1.0	Overlapped

A Fast Fourier Transform (FFT) analysis has been performed computing the Power Spectral Density (PSD) as Time-Integral Squared Amplitude (TISA) for each experiment in the two phases before and after applying the electrical stimulus, and the exemplar frequency of 1 kHz has been reported in Fig. 6 A. We can see how after the sample conditioning, the PSD increases by one order of magnitude in almost the entire frequency range. In Table 2 the values of PSD as TISA, obtained using a linear interpolant over the entire frequency range shown in Fig. 6 A, was calculated for all the experiments. We see how this quantity, besides the already discussed case of 1 kHz, seemingly fluctuates so that a specific rule to foresee the sample behaviour cannot be deduced.

One last visual element is provided in Fig. 6 B, to test our experimental results against memorisation features. The plot shows on a 2dimensional plane the parallel and perpendicular resistance components, and every frequency couple of points, representing the status of the system before and after the application of the electrical stimulus, is completed by a circle and an arrow identifying the temporal evolution. Experimental dots are shown with their statistical error bars (standard deviation), that can help in understanding how diverse and disjoint the two statuses can be. We can conclude that at the frequency of 1 kHz, the diversity of the two resistance paths is so high that it is possible to separate enough two statuses and effectively codify a binary information, using both components. At the frequency of 10 kHz, we cannot discriminate well the parallel channel, while the perpendicular is fine. At the frequency of 100 and 1000 kHz, we cannot discriminate well the perpendicular channel, while the parallel is fine. The composition of the transformation vectors shown in the top right inset, shows that the parallel resistance increases at low frequency and then decreases, while an opposite transformation is found for the perpendicular resistance. As already mentioned, low frequencies destroy the anisotropy of the colloid, higher frequencies contribute to increase the anisotropy along the stimulus axis.

One last comment about the learning procedure comes from the fast FTIR analyses and impedance spectroscopy measurements carried out on stimulated PANI NRs colloids (Fig. 7 A and B and Table S1).

As shown in Fig. 7 B and reported in Table 1, after the electric stimulus PANI NRs do not show structure and protonation level variation. However, the Nyquist plots (Fig. 7 A) highlight an increase in the system conductivity, which was also observed in the DC field, few

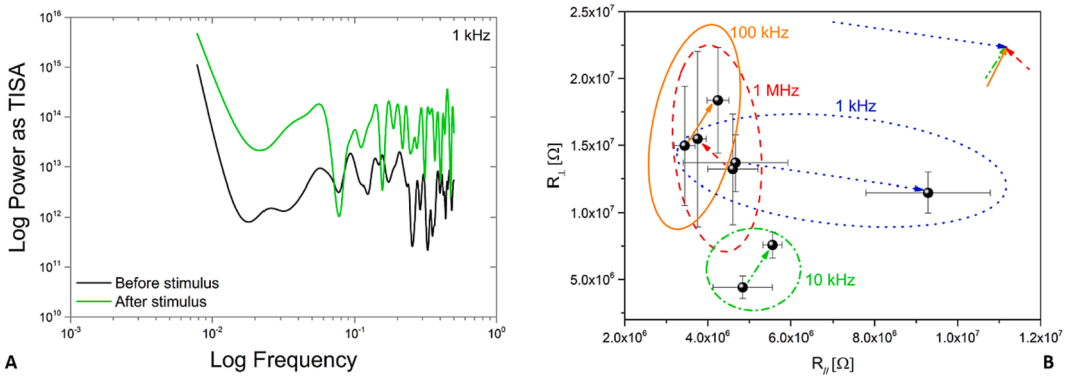

Fig. 6. (A) Power Spectral Density versus the logarithm of frequency, for the signals associated to the parallel resistance measures, before and after applying a stimulus at 1 kHz. (B) 2-dimensional plot of the parallel and perpendicular resistances measured in each experiment at the frequencies of 1 (dotted blue circle and arrow), 10 (dot-dashed green circle and arrow), 100 (continuous orange circle and arrow) and 1000 (dashed red circle and arrow) kHz. The top right inset shows the transformation vectors shifted and composed in the entire frequency evolution diagram. (For interpretation of the references to colour in this figure legend, the reader is referred to the web version of this article.)

Table 2
Comparison of PSD as TISA values derived from a linear interpolation in the frequency range 5 to 500 mHz (half of the sampling rate) and percent relative error, evaluated at all testing frequencies before and after submitting the stimulus.

Frequency [kHz]	Before stimulus	Err %	After stimulus	Err %
1	4.1×10^{12}	9	5.6×10^{13}	9
10	4.5×10^{12}	9	3.1×10^{12}	11
100	1.9×10^{12}	10	3.2×10^{12}	9
1000	4.3×10^{12}	9	1.7×10^{12}	10

seconds after submitting the stimuli.

As reported in literature [40], two types of doping can be applied to polyaniline (primary doping ad secondary doping) and both are responsible for the conductivity of the polymer.

Primary doping processes is related to both “redox doping” and “protonic doping”. The first process is associated to oxidizing or reducing agents’ removal or addition (electrons) that affect the oxidation state of the polymer, whereas the second process is related to the protonation of imines sites of the material, keeping unchanged the number of electrons associated with the polymer chains. Both these phenomena are completely reversible. In fact, de-doping leads to an inversion of some materials’ characteristics (e.g., conductivity). In contrast, the secondary doping process is a phenomenon generally caused by an apparent inert substance acting on primary doped-polymers. Unlike the other processes, it may persist, albeit to a reduced extent, even upon removal of the secondary doping.

On the basis of these premises, the variation in conductivity experienced by the material immediately after the electric stimulation can be directly associated to a modification on the secondary doping of PANI chains.

In fact, polyaniline can be considered as a polyelectrolyte: a macromolecule characterized by several charges (protonated imine groups and the corresponding anions of the dopant, here acetate ions). When exposed to apolar and/or aprotic solvents (e.g., chloroform), positive and negative ions associate in the chains forming ion pairs that favor a coil conformation of the molecular chain. In contrast, in the presence of polar and/or protic solvents (e.g., ethanol) the enhanced solvation of the charges lead to a more open and expanded molecular conformation (tail-like).

The achievement of the expanded conformation leads to rings twisting of the polymer backbone that causes a reduction of π-conjugation defects with an increase in the structure regularity and consequently in the conductivity.

According to literature [40], any effect that enhances the distance between positive and negative charges cause the expansion of the polymeric chains’ conformation and an increase in conductivity. Here, the application of an electric stimulus can be considered responsible for the polarization of both ethanol molecules and polymeric chains enhancing the distance between positive and negative charges with a beneficial effect on the materials conductivity. Once the polarization drops, the electrical equilibrium of the system is restored by Brownian motions in some seconds, but the morphological changes remain for a longer time scale, providing an increased DC resistance. This memory effect lasts for longer times and provides the observed learning. Therefore, it is possible to conclude that the AC stimulus positively affects the secondary doping of PANI NRs dispersed in ethanol.

This study represents the first evidence of the ability of an electrical

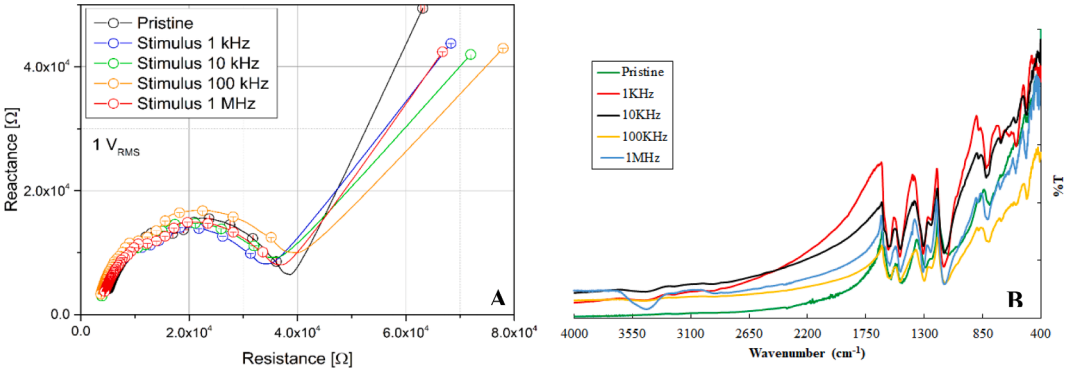

Fig. 7. Nyquist plots (A) and ATR-FTIR (B) spectra of pristine and stimulated PANI NRs colloids at 1KHz, 10 KHz, 100KHz and 1 MHz.

stimulation to affect the secondary doping of PANI-based materials and paves the way to new investigation for this surprising polymer.

Conclusions

To explain the experimental results, we can consider our study within a larger framework of colloids with programmable properties. The idea of using electromagnetic stimulation to change the electrical properties of colloids is not new. Wilke and Mülle demonstrated in 1933 that the conductivity of arsenic trisulfide colloids changed when stimulated with intermittent current [43]. The change in conductivity has been attributed to ion motions. In 2008, it was demonstrated [44] that the electrical conductivity of colloidal nano-suspensions exhibits complex behaviour that is dependent on particle size, electrical double layer thickness, suspension volume fraction, and ionic concentrations. A series of early 1900 s experimental studies [45–47] found that blood conductivity increases during coagulation because fibrin networks and erythrocytes are insulators. Similarly, but in reverse notation: PANI rods are conductive, and AC stimulus can be used to tune their secondary doping level. The resistance of the colloid droplet will decrease if they form parallel sheet-like pathways between the electrodes. Our hypothesis is supported by circumstantial evidence. When an electric field is applied parallel to the filaments' plane of motion, it exerts a mechanical force on the negatively charged actin filaments [48]. In this study, we demonstrated experimentally that a colloid of conductive polymer nanorods exhibits synapse-like behaviour, in other words, it is endowed with plasticity and its impedance level can be adjusted by repeating a stimulus, in this case a sinusoidal wave. We were able to programme the resistance in both directions parallel and perpendicular to the AC field lines by stimulating the colloid with AC. The effect of solvent intercalation and hydrogen bond loosening was also indicated by FTIR analyses performed before and after the electrical stimuli were applied. The ability of electrical stimulation to affect the secondary doping of PANI NRs colloids has been observed for the first time. The findings are consistent with our previous studies [49], in which we discovered that "entrainment" of copper-coated liquid marble filled with carbon nanotubes via periodic electrical pulses can cause their electrical resistance to rapidly switch between high and low resistance profiles when the polarity of stimulation is reversed. We recently demonstrated that a specific colloid, namely a water-based suspension of magnetite nanoparticles (ferrofluid), can perform memory computing as well as serve as an analogue memory [50]. In other words, we have demonstrated that when colloids are subjected to electric programming, they can memorise configurational information. If the droplets of the colloids are cascaded via amplifiers, the switching behaviour of the conductive polymer colloids can be used to implement networks of neuromorphic elements. Sequential logic operations and pattern recognition can also be performed by neuromorphic colloid droplets [50]. The findings also suggest that PANI NRs are a promising candidate for the development of unconventional computing systems for liquid robotics applications, where the ability to store and elaborate information with colloidal materials is critical for meeting the autonomy requirements of future exploration and inspection missions.

CRediT authorship contribution statement

Alessandro Chiolerio: Conceptualization, Data curation, Funding acquisition, Project administration, Resources, Supervision, Writing – original draft, Writing – review & editing. **Erik Garofalo:** Investigation. **Neil Phillips:** Investigation, Writing – review & editing. **Ermelinda Falletta:** Methodology, Validation, Visualization, Writing – review & editing. **Rodrigo de Oliveira:** Methodology, Validation, Visualization, Writing – review & editing. **Andrew Adamatzky:** Conceptualization, Investigation, Software, Writing – review & editing.

Declaration of competing interest

The authors declare the following financial interests/personal relationships which may be considered as potential competing interests: Alessandro Chiolerio reports financial support was provided by European Innovation Council.

Data availability

Data will be made available on request.

Acknowledgements

This project has received funding from the European Innovation Council And SMEs Executive Agency (EISMEA) under grant agreement No. 964388.

Appendix A. Supplementary data

Supplementary data to this article can be found online at https://doi.org/10.1016/j.rinp.2024.107501.

References

[1] Wong C, Yang E, Yan XT, Gu D. Autonomous robots for harsh environments: a holistic overview of current solutions and ongoing challenges. Systems Science Control Engineering 2018;6(1):213–9. https://doi.org/10.1080/21642583.2018.1477634.
[2] Chiolerio A, Quadrelli MB. Smart fluid systems: the advent of autonomous liquid robotics, advanced. Science 2017;4(7):1700036. https://doi.org/10.1002/advs.201700036.
[3] Kalita H, Thangavelautham J. Exploration of extreme environments with current and emerging robot systems. Current Robotics Reports 2020;1:97–104. https://doi.org/10.1007/s43154-020-00016-3.
[4] K. Groves, A. West, K. Gornicki, S. Watson, J. Carrasco, B. Lennox, MallARD: An Autonomous Aquatic Surface Vehicle for Inspection and Monitoring of Wet Nuclear Storage Facilities, Robotics, 2019, 8:2, 47, 10.3390/robotics8020047.
[5] Chiolerio A, Quadrelli MB. Colloidal Energetic Systems, Energy Technology 2018;7(5):1800580. https://doi.org/10.1002/ente.201800580.
[6] Chiolerio A, Adamatzky A. Tactile sensing and computing on a random network of conducting fluid channels. Flexible Printed Electron 2020;5:025006. https://doi.org/10.1088/2058-8585/ab906f.
[7] Bevione M, Garofalo E, Cecchini L, Chiolerio A. Liquid-state pyroelectric energy harvesting. MRS Energy Sustainability 2020;7:E38. https://doi.org/10.1557/mre.2020.39.
[8] Garofalo E, Cecchini L, Bevione M, Chiolerio A. Triboelectric characterization of colloidal TiO_2 for energy harvesting applications. Nanomaterials 2020;10(6):1181. https://doi.org/10.3390/nano10061181.
[9] Chiolerio A, Garofalo E, Bevione M, Cecchini L. Multiphysics-enabled liquid state thermal harvesting: synergistic effects between pyroelectricity and triboelectrification. Energ Technol 2021;9(10):2100544. https://doi.org/10.1002/ente.202100544.
[10] Chiolerio A, Garofalo E, Mattiussi F, Crepaldi M, Fortunato G, Iovieno M. Waste heat to power conversion by means of thermomagnetic hydrodynamic energy harvester. Appl Energy 2020;277:115591. https://doi.org/10.1016/j.apenergy.2020.115591.
[11] Garofalo E, Bevione M, Cecchini L, Chiolerio A. On the pyroelectric and triboelectric phenomena in ferrofluids. Advanced Materials Technologies 2022;7(10):2200127. https://doi.org/10.1002/admt.202200127.
[12] Chiolerio A, Draper TC, Jost C, Adamatzky A. Electrical properties of solvated tectomers: toward zettascale computing. Adv Electron Mater 2019;5(12):1900202. https://doi.org/10.1002/aelm.201900202.
[13] Adamatzky A, de Lacy Costello B, Melhuish C, Ratcliffe N. Liquid brains for robots. AISB Quarterly 2003:112:5.
[14] A. Adamatzky, Handbook of Unconventional Computing, 2021, WSPC Book Series in Unconventional Computing: Volume 1, DOI:10.1142/12232.
[15] N. Phillips, T. Draper, R. Mayne, D. Reynolds, A. Adamatzky, Marimo actuated rover systems, 2022, Journal of Biological Engineering, 16:3, 10.1186/s13036-021-00279-0.
[16] Phillips N, Draper TC, Mayne R, Adamatzky A. Marimo machines: oscillators, biosensors and actuators. J Biol Eng 2019;13:72. https://doi.org/10.1186/s13036-019-0200-5.
[17] Akhter S, Roberts J. Multi-Core Programming, volume 33. Oregon: Intel press Hillsboro; 2006.
[18] N. Raeisi Kheirabadi, A. Chiolerio, N. Phillips, A. Adamatzky, Learning in colloids: Synapse-like ZnO + DMSO colloid, 2023, 557, 126710, 10.1016/j.neucom.2023.126710.

[19] Jang J, Bae J, Lee K. Synthesis and characterization of polyaniline nanorods as curing agent and nanofiller for epoxy matrix composite. Polymer 2005;46(11):3677–84. https://doi.org/10.1016/j.polymer.2005.03.030.
[20] Wigge C, Hinssen H, Reiss G, Herth S. Positioning and stretching of actin filaments by electric fields. Appl Phys Lett 2010;96:243703. https://doi.org/10.1063/1.3455338.
[21] Abdelraheem A, El-Shazly AH, Elkady MF. Characterization of atypical polyaniline nano-structures prepared via advanced techniques. Alex Eng J 2018;57–4:3291–7. https://doi.org/10.1016/j.aej.2018.01.012.
[22] Y. Atassi, M. Tally, M. Ismail, arXiv:0809.3552v1 [cond-mat.mtrl-sci].
[23] Falletta E, Ferretti AM, Mondini S, Evangelisti C, Capetti E, Olivetti ES, et al. Size-dependent catalytic effect of magnetite nanoparticles in the synthesis of tunable magnetic polyaniline nanocomposites. Chem Pap 2021;75(10):5057–69. https://doi.org/10.1007/s11696-021-01604-z.
[24] Salaneck WR, Liedberg B, Inganäs O, Erlandsson R, Lundström I, Macdiarmid AG, et al. Physical characterization of some polyaniline, (øN)x. Mol Cryst Liq Cryst 1985;121(1–4):191–4. https://doi.org/10.1080/00268948508074860.
[25] Dhivya C, S. Anbu Anjugam Vandarkuzhali, N. Radha,. Antimicrobial activities of nanostructured polyanilines doped with aromatic nitro compounds. Arab J Chem 2019;12–8:3785–98. https://doi.org/10.1016/j.arabjc.2015.12.005.
[26] C. Cionti, C. Della Pina, D. Meroni, E. Falletta, S. Ardizzone, Photocatalytic and Oxidative Synthetic Pathways for Highly Efficient PANI-TiO2 Nanocomposites as Organic and Inorganic Pollutant Sorbents, Nanomaterials, 2020, 10:3, 441, 10.3390/nano10030441.
[27] Bianchi CL, Djellabi R, Della Pina C, Falletta E. Doped-polyaniline based sorbents for the simultaneous removal of heavy metals and dyes from water: unravelling the role of synthesis method and doping agent. Chemosphere 2022;286(3):131941. https://doi.org/10.1016/j.chemosphere.2021.131941.
[28] C. Della Pina, M. A. De Gregorio, P. Dellavedova, E. Falletta, Polyanilines as New Sorbents for Hydrocarbons Removal from Aqueous Solutions, Materials, 2020, 13:9, 2161, 10.3390/ma13092161.
[29] Yang C, Fang Z, Zhang P. UV-vis spectra of polyaniline doped with camphor sulfonic acid in different organic solvents. J Cent South Univ Technol 1999;6:127–9. https://doi.org/10.1007/s11771-999-0014-6.
[30] Alam M, Alandis NM, Ansari AA, Shaik MR. Optical and electrical studies of polyaniline/ZnO nanocomposite. J Nanomater 2013;147:147. https://doi.org/10.1155/2013/157810.
[31] Pouget JP, Jozefowicz ME, Epstein AJ, Tang X, MacDiarmid AG. X-ray structure of polyaniline. Macromolecules 1991;24(3):779–89. https://doi.org/10.1021/ma00003a022.
[32] Wanga J, Zhang S. Synthesis of polyaniline-sulfur composites with different nanostructures via an interfacial emulsification method and a micelle template method and their properties. RSC Adv 2020;10(19):11455–62. https://doi.org/10.1039/D0RA00122H.
[33] Wu F, Chen J, Li L, Zhao T, Chen R, Wang Y, et al. Improvement of rate and cycle performence by rapid polyaniline coating of a MWCNT/SULFUR cathode. J Phys Chem C 2011;115(49):24411–7. https://doi.org/10.1021/jp207893d.
[34] Hsini A, Naciri Y, Laabd M, Bouziani A, Navío JA, Puga F, et al. Development of a novel PANI@WO3 hybrid composite and its application as a promising adsorbent for CR(VI) ions removal, journal of environmental. Chem Eng 2021;9(5):105885. https://doi.org/10.1016/j.jece.2021.105885.
[35] Li M, Yin W, Han X, Chang X. Hierarchical nanocomposites of polyaniline scales coated on graphene oxide sheets for enhanced supercapacitors. J Solid State Electrochem 2016;20:1941–8. https://doi.org/10.1007/s10008-016-3202-y.
[36] Wang Y, Jing X. Formation of polyaniline nanofibers: a morphological study. J Phys Chem B 2008;112(4):1157–62. https://doi.org/10.1021/jp076112v.
[37] F. Zeng, Z. Qin, B. Liang, T. Li, N. Liu, M. Zhu, Progress in Natural Science: Materials International 25, 512-515.
[38] Nadagouda MN, Varma RS. Green approach to bulk and template-free synthesis of thermally stable reduced polyaniline nanofibers for capacitor applications. Green Chem 2007;9(6):632–7. https://doi.org/10.1039/B614633C.
[39] Wilke E, Müller R. Einwirkung elektrischer wellen auf kolloide. Kolloid-Zeitschrift 1933;65:257–60. https://doi.org/10.1007/BF01824485.
[40] Alan G. MacDiarmid and Arthur J. Epstein, Secondary doping in polyaniline, Synthetic Metals, 69 (1995) 85-92.
[41] de Medeiros DWO, da Trindade Neto CG, dos Santos DES, Pavinatto FJ, dos Santos DS, Oliveira Jr ON, et al. Preparation and characterization of PAni-PMMA dispersions. J Dispers Sci Technol 2005;26(3):267–73. https://doi.org/10.1081/DIS-200049560.
[42] Ziadan KM, Saadon WT. Study of the electrical characteristics of polyaniline prepared by electrochemical polymerization. Energy Procedia 2012;19:71–9. https://doi.org/10.1016/j.egypro.2012.05.184.
[43] Tarachiwin L, Kiattibutr P, Ruangchuay L, Sirivat A, Schwank J. Electrical conductivity response of polyaniline films to ethanol–water mixtures. Synth Met 2002;129(3):303–8. https://doi.org/10.1016/S0379-6779(02)00112-1.
[44] Chakraborty S, Padhy S. Anomalous electrical conductivity of nanoscale colloidal suspensions. ACS Nano 2008;2(10):2029–36. https://doi.org/10.1021/nn800343h.
[45] Frank RT. A note on the electric conductivity of blood during coagulation. American Journal of Physiology-Legacy Content 1905;14(5):466–8.
[46] Wilson T. The conductivity of blood in coagulation. Biochem J 1907;2(7–8):377–82. https://doi.org/10.1042/bj0020377.
[47] Mellanby J. The coagulation of blood. J Physiol 1908;38(1):28–112. https://doi.org/10.1113/jphysiol.1908.sp001297.
[48] Riveline D, Ott A, Jülicher F, Winkelmann DA, Cardoso O, Lacapère JJ, et al. Acting on actin: the electric motility assay. Eur Biophys J 1998;27:403–8. https://doi.org/10.1007/s002490050147.
[49] Mayne R, Draper TC, Phillips N, Whiting JG, Weerasekera R, Fullarton C, et al. Langmuir 2019;35(40):13182–8. https://doi.org/10.1021/acs.langmuir.9b02552.
[50] Crepaldi M, Mohan C, Garofalo E, Adamatzky A, Szaciłowski K, Chiolerio A. Adv Mater 2023:2211406. https://doi.org/10.1002/adma.202211406.

Alessandro Chiolerio is a research scientist at the Bioinspired Soft Robotics laboratory of Istituto Italiano di Tecnologia, Genova, Italy and a visiting professor at the Unconventional Computing Laboratory, Department of Computer Science, University of the West of England, Bristol, UK. He is exploring the complexity of cybernetic systems, including liquid state autonomous robots and electron devices, living organism ensembles, colloids and fogs. Founder of two technological spin-offs and CSO of a third one, he is author and co-author of more than 130 scientific articles and 34 patents, and has raised over € 10.5 million in research/startup funding based on his own ideas.

Erik Garofalo is Space Engineer and researcher at Soft Bioinspired Robotics laboratory of Istituto Italiano di Tecnologia, Genova, Italy. He was Visiting Researcher at California Polytechnic State University and University of the West of England. He is currently investigating novel soft robotic systems at the liquid state for space and terrestrial exploration of harsh environments, having experience in space exploration and rocket science, robotics, energy recovery and conversion. He is author/co-author of 10 scientific articles in peer-reviewed journals, 5 proceedings in international conferences and 1 patent.

Neil Phillips has over 20 years of industrial manufacturing and innovation expertise. He is passionate about discovering unconventional solutions to overcome enduring technical challenges. His research interests include bio-computing, biomimicry, liquid marbles, Marimo, contactless cell mapping, bio-reactors, bio-sensing, slime mould and high temperature superconductors. He currently works at the University of the West of England as a post-doctoral researcher, with a focus on unconventional computing. He is author/co-author of 50 publications and 6 patents.

Ermelinda Falletta is a researcher at the Department of Chemistry of the University of Milan. She has over ten years of experience in the development of innovative environmentally friendly approaches for the preparation of intrinsically conducting polymers and their composites and in their application in the field of environmental remediation and piezoresistors. Her research field also extends to the design of heterogeneous catalysts for emerging pollutants photodegradation. She is author/co-author of 80 publications, 3 books, 8 book chapters, and 2 patents.

Rodrigo de Oliveira Rodrigo is a chemist with PhD in Chemistry (Advisor: Prof André Galembeck) from Federal University of Pernambuco, Brazil. During the PhD he did a sandwich stage at the School of Chemistry of the University of Bristol, UK, under supervision of Prof Julian Eastoe. He did propose a new class of surfactants with photoreactive headgroups in order to make metal and metal oxide nanoparticles in reverse micelles. Actually he is Professor Associado A at the State University of Paraiba (since 2012), Brazil, where he is running the Physical-Chemistry of Materials Group (PCM) dealing with reuse of polystyrene to make functional foams doped with metal nanoparticles for environmental, catalytic and energy applications; modification of synthetic and natural clays from Paraiba State to make new materials for agricultural and energy applications and also colloidal chemistry and its electrical characterization. In 2017 he was awarded the Benjamin Meaker Visiting Professorship of the University of Bristol under supervision of Dr Jeroen van Duijneveldt, dealing with clay modifications to induce arresting using polyphosphates. Since 2022 he is in a postdoc stage under supervision of Prof Alessandro Chiolerio at IIT-Genova, working on self-healing skins for soft robots.

Andrew Adamatzky is Professor of Unconventional Computing and Director of the Unconventional Computing Laboratory, Department of Computer Science, University of the West of England, Bristol, UK. He does research in molecular computing, reaction-diffusion computing, collision-based computing, cellular automata, slime mould computing, massive parallel computation, applied mathematics, complexity, nature-inspired optimisation, collective intelligence and robotics, bionics, computational psychology, nonlinear science, novel hardware, and future and emergent computation. He authored seven books, mostly notable are 'Reaction-Diffusion Computing', 'Dynamics of Crow Minds', 'Physarum Machines', and edited twenty-two books in computing, most notable are 'Collision Based Computing', 'Game of Life Cellular Automata', 'Memristor Networks'; he also produced a series of influential artworks published in the atlas 'Silence of Slime Mould'. He is founding editor-in-chief of 'J of Cellular Automata' and " J of Unconventional Computing' and editor-in-chief of "J Parallel, Emergent, Distributed Systems' and 'Parallel Processing Letters'.